Available online at www.sciencedirect.com

ScienceDirect

Ciência & Tecnologia dos Materiais 27 (2015) 92–99

Ciência & Tecnologia dos MATERIAIS

http://ees.elsevier.com/ctmat

Special Issue IJSI 2014

Influence of the kissing bond defect on the fatigue life in friction stir welds of 2024 aluminium alloy

Roman Růžek, Martin Kadlec*, Lucie Nováková

VZLU - Aerospace Research and Test Establishment, Beranovych 130, 199 05 Prague, Czech Republic

Abstract

Static and fatigue experiments were performed on friction stir (FS) welds in 2024-T3 aluminium alloys to investigate the influence of kissing bond (KB) flaws on the static strength and fatigue life of the FS welds. Different categories of FS welded plates were manufactured: a flaw-free plate and FS welded plates with different levels of KB size. The effects of the KB flaws on tensile and fatigue properties of AA2024-T3 specimens extracted from the plates were quantitatively evaluated with respect to the flaw-free weld. The various levels of KB flaw size were investigated with the aim of determining a flaw size that does not affect the fatigue life of the joined 6.35-mm-thick plates. The critical value for the KB geometry seems to be below 400 µm in depth based on the influence on the fatigue life for the investigated categories. The fatigue life of welds with KB flaws of 615 µm average depth was approximately seven times shorter than for flaw-free welds. The test results were supported by metallographic analyses and provide a baseline for definition of the flaw detection requirements related the sensitivity of non-destructive equipment.

Keywords: fatigue strength; friction stir welding; kissing bond; 2024 aluminium alloy; aerospace vehicles.

1. Introduction

Friction Stir Welding (FSW) is a high-performance joining technique used primarily for aluminium alloys which offers excellent joint performance and reproducibility [1]. Although the FSW technique was initially developed for Al-alloys, it also has great potential for welding of Mg-, Cu-, Ti-, Al-alloy matrix composites, lead, some steels, stainless steels, thermoplastics and different material combinations [2–7]. FSW technology contributes to increased joining speed, higher stress tolerance, better reproducibility and longer service life when compared to common riveting methods [8]. This is important to sectors, such as aerospace [9,10] and automotive [11], where fatigue performance is particularly crucial. The mechanical properties of FSW welds are better in comparison with traditional welding techniques because it avoids the necessity for large temperature gradients [12,13]. In recent years, several investigations have been conducted on the fatigue properties of friction stir welded joints [14,15]. In a comparison study, it was observed that Metal Inert Gas (MIG)-pulse and Tungsten Inert Gas (TIG) welds presented both lower static and fatigue strengths than friction stir welds [16].

Wider use of FSW among industrial applications is limited by the ability to detect flaws of a relatively small geometry. This problem limits the adoption of FSW for joining of critical components. Although the vast majority of friction stir welds will be free of flaws, it is not always possible to assume that they are.

Material flow behaviour is one of the most important factors that influence the quality of the FS weld. The movement of the rotating tool along the welding direction forms the joint. The tool geometry (shoulder

* Corresponding author.

E-mail address: kadlec@vzlu.cz (M Kadlec)

http://dx.doi.org/10.1016/j.ctmat.2015.03.012

diameter, tool shape), rotational speed, feed rate, vertical pressure and external cooling affect the heat generated in the material. Those effects influence the material structure and material properties of the weld [17]. The strong relation between the grain size and the mechanical properties was demonstrated in [18].

A typical weld defect occurring in joints made with FSW is the kissing bond (KB) defect. A kissing bond is a specific type of solid-state bonding defect where two previously separate or separated regions of the material are in contact with little or no metallic bond present. Kissing bond flaws can occur in the root of the weld; in this situation, the materials are in close contact but are not chemically or mechanically bonded [19]. KBs cause issues in FSW because they can reduce the fatigue performance of joints [20] and currently are highly difficult to detect using existing non-destructive techniques (NDT) [21]. The influence of KB flow geometry on reduction of the fatigue behaviour of AA7475 T7351 material was discussed in [22]. A kissing bond size of 315 μm was demonstrated to be insignificant with respect to the fatigue and static behaviour for AA7475 T7351 plate material with a thickness of 6.35 mm [22].

The overall aim of the project addresses the development of NDT systems that will be able to detect small KB flaws. As part of the project, the current work addresses the definition of an acceptable flaw for which the flaw size has no influence on the mechanical properties of joints. Simultaneously, the KBs with such size must be detectable by NDT systems. Fatigue durability is the main parameter that must be taken into account for the economical and reliable operation of any structure. In general, it is assumed that no manufacturing flaws are present, but in reality, each structure contains manufacturing defects of a certain size. This paper is focused on assessing the influence of the KB defect geometry on the mechanical (static and fatigue) properties of an FSW joint in AA2024-T3 material.

2. Materials and methods

2.1. Material and mechanical test methods

Plates of AA2024-T3 with thickness of 6.35 mm were cut and welded by FSW. The chemical composition of the AA2024-T3 plates was: 4.3 wt% Cu, 1.5 wt% Mg, 0.70 wt% Mn, 0.5 wt% Si, 0.3 wt% Fe, and 0.2 wt% Zn; the balance was Al. Using various levels of the tool probe stick, different KB flaw sizes and a flaw-free FSW joint were manufactured according to Table 1. No post-weld heat treatment was performed. Two types of test specimens were machined from larger butt-welded plates of 1000 mm × 300 mm × 6.35 mm each. The FSW butt joints were produced by TWI. The specimen design for static tension evaluation described in the AWS D17.3 standard [23] was adopted (Fig. 1a). Fatigue test specimens with stress concentration factor K_t = 1 were machined according to the EN 6072 standard [24] (Fig. 1b). The direction of the FSW butt joint was perpendicular to the longitudinal axis of the specimens and the load introduction direction.

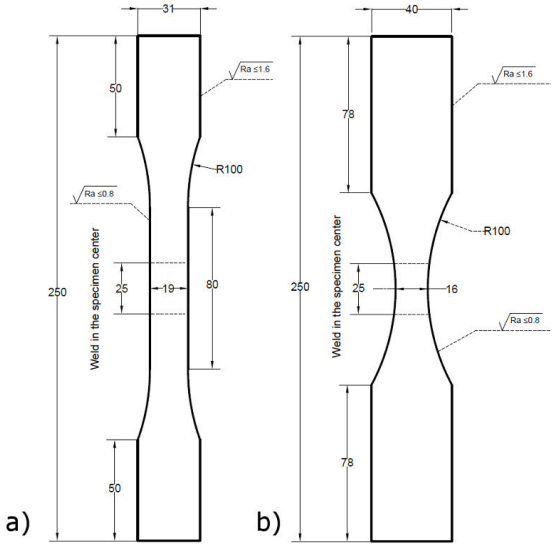

Fig. 1. Specimen geometry for a) static and b) fatigue testing.

The test matrix (Table 1) was established to determine a specific KB size that will not significantly decrease the fatigue performance of the FSW joint. Therefore, a flaw-free FSW and two levels of flaw sizes within the welds were compared and evaluated. The minimum number of test specimens per plate was determined by the respective standards and the availability of material.

Static tensile tests were conducted using an Instron mechanical test machine with a capacity of 100 kN (Fig. 2a). The yield strength, tensile strength, and elongation values were evaluated from the static tests. The elongation was measured at a gauge length of L_o = 50 mm. Fatigue tests were carried out using a hydraulic fatigue test machine IST Hydropuls Sinus

with a capacity of 100 kN (Fig. 2b). A sinusoidal load-time function was employed with the two stress ratios $R = \sigma_{min} / \sigma_{max}$. The stress ratios were set to 0.05 and 0.6 at several different maximum stress levels σ_{max}. The test frequency range was between 5 Hz and 15 Hz and tests were performed in laboratory air. The fatigue data of the S–N curves were expressed as the maximum stress $(\sigma_{net})_{MAX}$ (MPa) versus the corresponding life to failure (i.e., number of cycles). The stress was calculated from the net cross-section at the narrowest part of the specimen. Assessment of the fatigue behaviour of the welds was obtained by applying statistical analysis to produce fatigue strength data as represented in the S-N diagrams.

Table 1. Test matrix of specimens manufactured from 3 welded plates.

Plate	Static test number of tens. spec.	Fatigue number of fatigue spec.	Measured mean KB size
FSW flaw free	6	14	-
FSW large KB	6	14	(615 ±45) µm
FSW small KB	6	14	(450 ±65) µm

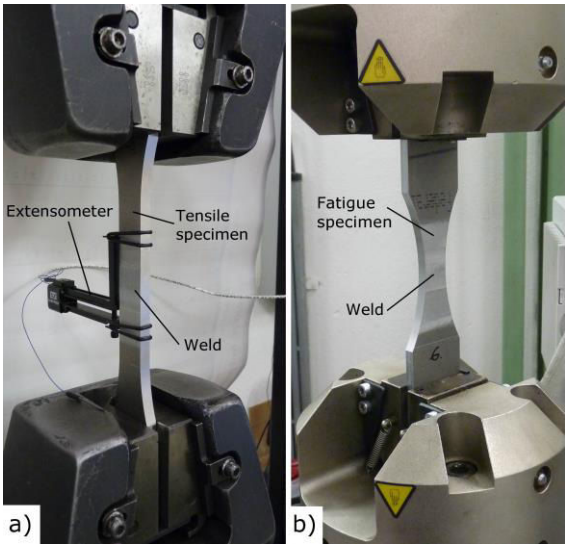

Fig. 2. a) Tensile (AWS D17.3) and b) fatigue (EN 6072) test set-up.

A fatigue curve was generated by performing a series of experiments at prescribed maximum stress levels. The load levels were chosen so that the results would be regularly positioned on the S-N curve between at least 10^4 and 3.10^6 cycles in compliance with the EN 6072 standard [24]. In cases where there was no failure at 3.10^6 cycles, specimens were tested again at the same load level up to 8.10^6 cycles at least. In cases where there was still no failure, the specimen was tested again at a higher load level that had been shown to lead to failure before 10^5 cycles. The exact KB size was determined using an optical microscope for each specimen from the fractured surface in cases where failed in the KB, or from the specimen edge in cases where it failed out of the KB. Table 1 presents mean values and sample standard deviations of measured KB depths along the welds in the direction perpendicular to the surface.

2.2. Fractographical analyses

To determine the cause of failure for the specimens, metallography, indentation, and fractography analyses were conducted. Several specimens from each plate were cut to evaluate the weld microstructure, the distribution of the grains and the geometry of the flaws. The samples were prepared using a standard metallographic method. The final polishing was performed using the MasterPrep Alumina Polishing Suspension (0.05 µm). The microstructure of the samples was revealed by Barker's electrolytic etching method with subsequent optical microstructural contrasting in polarized light using an Olympus GX51 optical microscope. Magnifications of 50×, 100×, 200×, 500×, and 1000× were used in the analyses.
A more detailed microfractographic analysis was used to understand fatigue crack growth direction and initiation. The overview pictures of crack propagation were taken by a Canon 500D camera with a macro objective. The microfractographic analyses of fracture surfaces were carried out using a TESCAN 3SBU Scanning Electron Microscope (SEM) set to secondary electron imaging mode. The high vacuum mode with a high voltage value of 30 kV was used for the evaluation. The adjusted microscopy parameters for these pictures are noted under the pictures. Vega TC microscope operating software was used.

3. Results and discussion

3.1. Weld structure

The cross-sectional visualisation of a plate with a 450 µm flaw is presented in Fig. 3a. The thermo-mechanically affected zone (TMAZ) is the region around the weld nugget. The border is evident on both

the retreating and advancing side composed of elongated grains. The heat affected zone (HAZ) extends further beyond the TMAZ. Fig. 3b shows a KB detail from the lower part of the nugget.

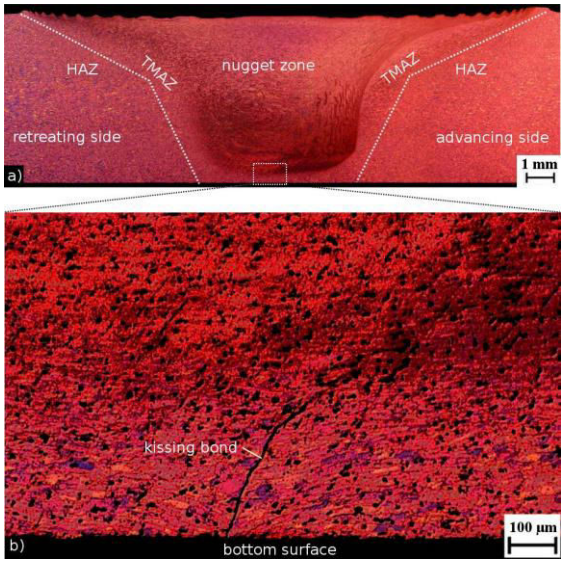

Fig. 3. Metallographic analysis of a kissing bond size (small KB of 450 µm). a) Overview picture around the weld nugget. b) Detail of a KB flaw.

3.2. Quasi-static tensile test results

Mean values of specific static tensile chracteristics for each plate are presented in Table 2. The stress-strain curves are presented in Fig. 4. The selected characteristics were: tensile strength (maximum stress), elongation (maximum achieved strain before fracture), and yield strength (offset stress point at 0.2% of the strain – $R_{p0.2}$). Compared to the flaw-free weld, the other measured characteristics (i.e., tensile strength and elongation) of the welded specimens were decreased.

Table 2. Static tensile test results including sample standard deviations.

	FSW – flaw free	FSW – small KB 450 µm	FSW – large KB 615 µm
R_m (MPa)	421.3 ±3.2	403.8 ±8.1	354.2 ±2.1
$R_{p0.2}$ (MPa)	291.3 ±2.5	292.7 ±2.5	293.1 ±1.6
Elong. (%)	11.6 ±1.0	8.8 ±1.4	2.6 ±0.4

The results show that the presence of a KB caused a decrease in strength by 4% and 16% for 450 µm and 615 µm, respectively, in comparison to the flaw-free FSW. The yield strength had no significant change for the flawed welds. There is also a significant decrease of elongation by 24% and 77% for 450 µm and 615 µm KB, respectively. The elongation was significantly influenced by zone of failure initiation (base material / HAZ / KB).

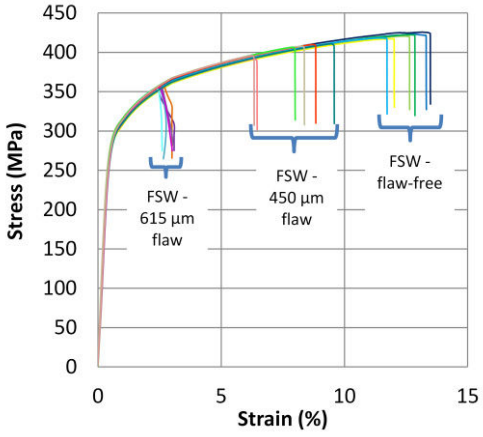

Fig. 4. Stress-strain curves for static testing of the FSW joints without and with a kissing bond flaw.

3.3. Fatigue testing results

Fatigue durability is an important selection criterion for aerospace materials because of the cyclic stresses that occurs in an aircraft structure. Focusing on aerospace applications, the influences of the welding and the presence of KB flaws were determined by fatigue testing. The scope of the experiment was to establish the fatigue curve in compliance with the EN 6072 standard. A linear regression model used for the failed specimens is represented by Eq. 1:

$$\log(N_f) = A_1 + A_2 \cdot \log(\sigma_{net})_{MAX}, \quad (1)$$

where A_1 and A_2 represent the regression constants.
The results for stress ratio R = 0.05 are shown in graphical form in Fig. 5. The real area of interest for structures is the long life regime ($N>10^6$ cycles). The advanced aluminium alloys used in the aerospace industry typically have two main regions. Some of these show a relatively sharp fatigue limit or two very different slopes of the S-N curve in a log-log data presentation (in comparison to high/low applied stresses). A plateau in the stress–fatigue life relationship occurs such as that for the other metals (typically a high strength steel). The 2024 T3 plate

material investigated in this paper is a representative of these materials. This is obvious from data presented in this paper. Data was therefore calculated using a statistical evaluation to determine the fatigue curve up to 2.10^6 cycles. For longer lives the fatigue limit can be found. Although determination of the fatigue limit was not the aim of this work, the fatigue limit can be roughly estimated on the basis of the presented data.

The fracture for the flaw-free welded specimens tested at $R = 0.05$ occurred on the advancing side for all the specimens, directly from the surface step caused by the tool in the transition of the TMAZ and base metal. The fatigue limit of $(\sigma_{net})_{MAX}$ = 100 MPa can be estimated. The FSW with the 615 µm KB caused significant decrease of the fatigue life (7 times shorter compared to flaw-free specimens), and the fatigue limit of $(\sigma_{net})_{MAX}$ = 65 MPa can be estimated. The decrease was caused by the crack initiation directly from the KB. On the contrary, the third curve for FSW with a 450 µm KB flaw (red triangle point in Fig. 5) does not show a significant difference compared to the flaw-free weld in terms of fatigue life within the measured range of stress. The fracture was also similar to the flaw-free specimens, occurring on the transition area of the advancing side. However, crack initiation from the KB in some specimens (two results) caused lower fatigue life. These specimens were not considered in the linear regression because of the deviation of the failure mode. Fig. 5 presents the complete set of fatigue results, including all relevant elements. This finding means that the criterion for insignificant flaw size and simultaneously the minimum detectable size for a non-destructive technique will be below 400 µm. The optimum value will have to be found by additional experiments. The high variation of KB sizes along the weld length was also apparent and caused the scatter in the fatigue life and failure modes.

The material was loaded during fatigue cycling below the yield strength ($R_{p0.2}$ = 300 MPa). It should be noted that the welds were not treated by post-weld heat treatment and that the residual stresses are presented. Residual stress varies according to welding parameters and restraining during welding. If this stress were to be relieved, the fatigue lives would be increased. The specific increase of lives cannot be estimated without proper residual stress measurements [25].

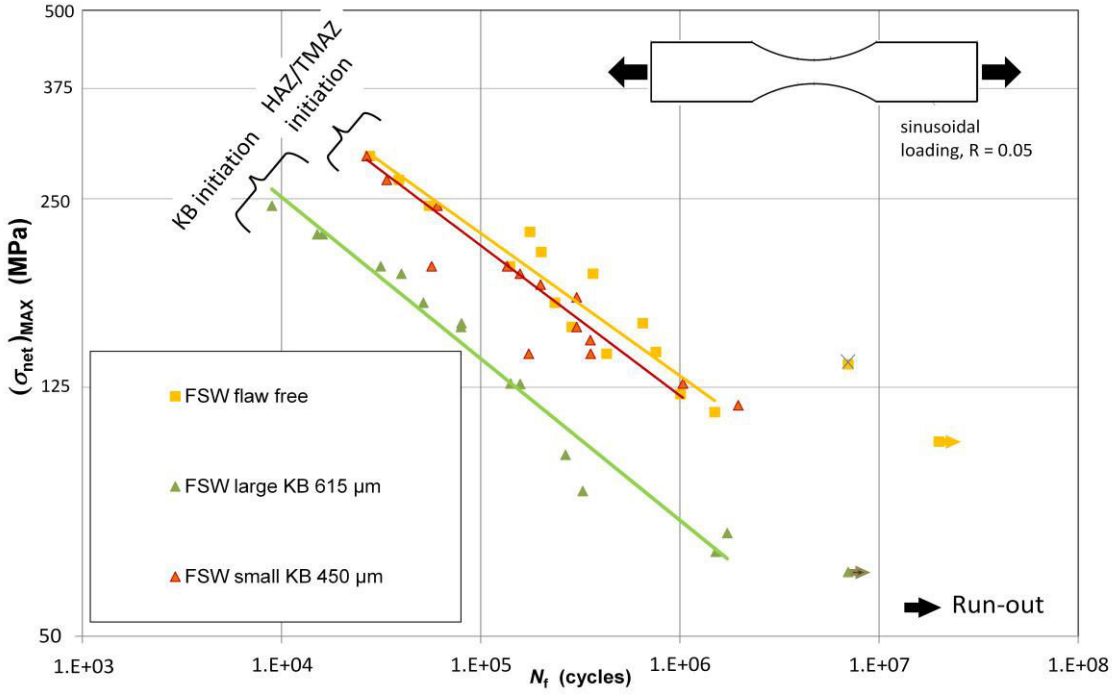

Fig. 5. Fatigue test results of specimens from flaw-free FSW, and FS welds with 2 different mean sizes of kissing bonds. Part of the small 450 µm flaw specimens was comparable to flaw free specimens.

Figure 6 shows in graphical form the fatigue results obtained for load ratio $R = 0.6$. The 450 µm KB flaws caused shorter fatigue lives than the flaw-free FSW specimens (decreasing approximately 40%). However, only a small number of specimens were evaluated which made the difference not statistically significant. There was also a change in fracture mode in comparison to the load ratio level of 0.05. The higher asymmetry of $R = 0.6$ caused a change of the fracture that occurred on the retreating side as opposed to that of the lower R. The 650 µm KB flaw caused a significant decrease in fatigue life similar to that observed for the low load ratio, with initiation occurring from the KB flaw (decreasing approximately by one order of magnitude compared with the flaw-free specimens).

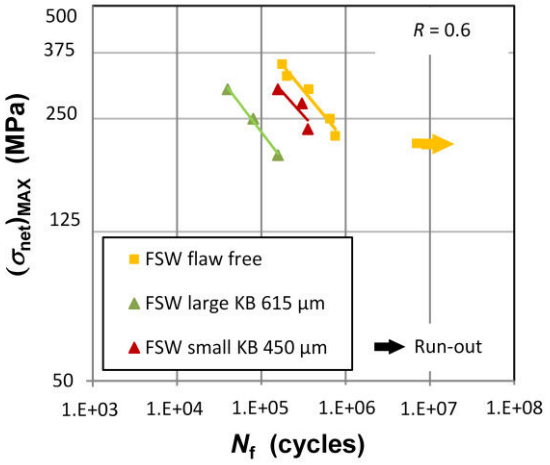

Fig. 6. Fatigue test results for $R = 0.6$ of specimens from flaw-free FSW, FSW with 615 µm KB, and FSW with 450 µm KB.

3.4. Macrofractography

The failure mechanisms of selected fatigue specimens were analysed in more detail using optical and scan electron microscopy. One of the fracture modes involved crack initiation along the width of the specimens directly from the surface step in the transition area between the weld zone and base material (Fig. 7a). This mode occurred for the flaw-free weld and also for the welds with relatively small flaws as noted in Table 3.

The side of crack initiation depended on the loading asymmetry; for $R = 0.05$, the fracture occurred on the advancing side, and for $R = 0.6$ on the retreating side. Multiple fatigue crack initiation was visible over the whole fracture surface width along the transition step (Fig. 7b). This proves that the surface step of the transition had the effect of a notch. In terms of macroscopic observation, no differences in the propagation mechanism were found. The crack propagated with higher growth rate in the corners of the specimens.

Table 3. Fracture locations observed for AA2024 and mean values of the KB size including standard deviation measured along the weld.

Plate	Fatigue crack initiation		Mean measured KB size
	HAZ/TMAZ transition	Kissing bond	
FSW flaw free	$R = 0.05$ Adv. / $R = 0.6$ Retr.		-
FSW large KB		X	(615 ±45) µm
FSW small KB	$R = 0.05$ Adv. / $R = 0.6$ Retr.	X	(450 ±65) µm

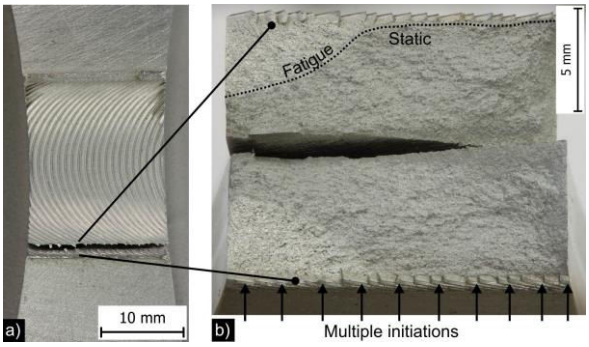

Fig. 7. Fatigue fracture initiation on the retreating side of the weld: a) the upper part of weld; b) fracture surface with multiple initiations and higher crack growth rate in a specimen corner.

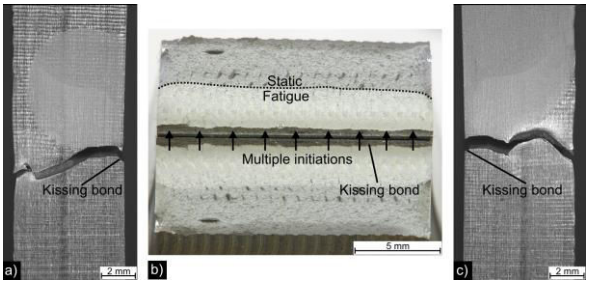

Fig. 8. The fatigue fracture initiation from the KB flaw: a) left the side view; b) fracture surface with multiple initiation form; c) right side view.

The second fracture mode was multiple fatigue crack initiation from the KB flaw (Fig. 8). It appeared on certain specimens with KB flaws. Specimens manufactured from some plates with relatively large flaws failed exclusively by this type of fracture (Table 3). Fig. 8 also shows side views of the fracture

revealing a nonplanar fracture surface near the specimen free surfaces caused by the shear stress in the plain stress region.

3.5. Microfractography

Five representative fatigued specimens were chosen for the detailed fractographic analysis using a SEM. One sample of FSW without a kissing bond flaw, three samples with small kissing bond flaws (among them two which had different fatigue lives) and one sample with a large kissing bond flaw were chosen. The following micromorphological characteristics were found on the observed fracture surfaces using the scan electron microscopy.

Fig. 9 shows a sample with a flaw-free FSW. The initiation occurred on the advancing side of the HAZ/TMAZ transition in the upper side of the weld. The subfigures show multiple crack initiation featured by ratchet marks that initiated from the trailing grooves. The deep surface trailing grooves created by the tool shoulder had the effect of notches that initiated multiple cracks. Cracks propagated by the striation mechanism until final fracture featured ductile dimples. The striations represent local crack-growth increments per cycle and appears as parallel markings perpendicular to the local crack growth.

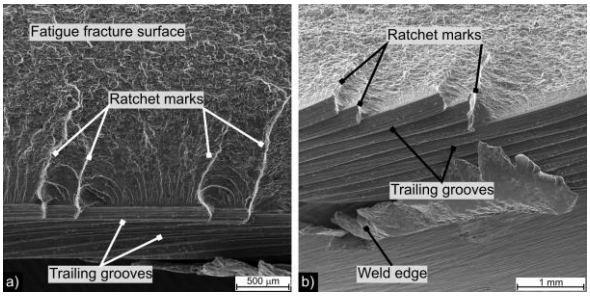

Fig. 9. Fatigue crack initiation from the surface grooves in the HAZ/TMAZ transition on the advancing side observed by scan electron microscopy: a) fracture surface top view; b) angled view.

Fig. 10 shows the second failure mode of fatigue specimens. Multiple crack initiation was featured by ratchet marks that initiated from the kissing bond notch. Cracks propagated by the striation mechanism until final fracture featured ductile dimples.

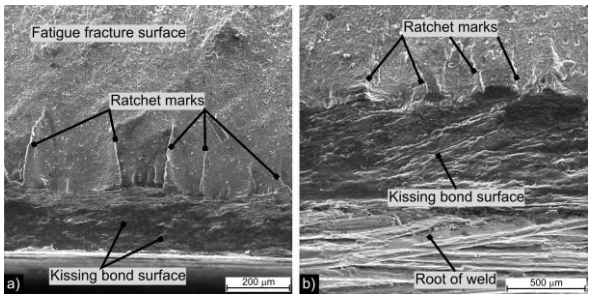

Fig. 10. Fatigue crack initiation from the KB flaw notch observed by electron microscopy: a) fracture surface top view; b) angled view.

4. Conclusions

This study investigated the static and fatigue properties of friction stir welded AA2024-T3 plates to determine the critical size of a kissing bond flaw that will not significantly decrease the weld performance. No KB is acceptable in aerospace structures, but at the same time the presence of KB cannot be excluded during serial production. Therefore, a flaw size criterion must be defined to provide requirements on the detectability of the flaws using non-destructive methods. The testing on a series of FS welded joints that included various kissing bond sizes provided the following results:

- The flaw affects the material structure locally, which leads to a decrease in the mechanical properties. Compared to the flaw-free weld, the tensile strength and elongation of the FS welded specimens are lower depending on the flaw geometry.
- The 615-µm kissing bond caused a significant decrease in the fatigue life and initiation from the kissing bond was observed in all cases.
- Some FSW specimens with 450 µm KB in depth failed out of the KB, in the HAZ/TMAZ area, and the fatigue behaviour was comparable with flaw-free FSW specimens. This finding means that the criterion and simultaneously the minimum detectable size for AA2024-T3 alloy must be below 400 µm.

Acknowledgments

The authors would like to acknowledge TWI for supplying the welded test plates used in this work. The research leading to these results has received funding from the European Community's Seventh Framework

Programme (Theme SME-2012-1) for the SMEs research under grant agreement n° 315436.

References

[1] W.M. Thomas et al., inventor, Welding Inst, assignee. Improvements relating to friction welding. Patent Application PCT/GB1992/002203, 1992 Nov 27.
[2] G. Çam., Int. Mater. Reviews 56 (2011) 1.
[3] C.J. Dawes, W.M. Thomas., Weld. J. 75(3) (1996) 41.
[4] W.B. Lee, Y.M. Yeon, S.B. Jung., Mater. Sci. Eng. A 355 (2003) 154.
[5] P.L. Threadgill, A.J. Leonard, H.R. Shercliff, P.J. Withers. Int. Mater. Rev. 54(2) (2009) 49.
[6] P. Bělský. Innovative Welding Technologies for Joining Al Alloy 6082-T6, Czech Aerospace Proceedings 2 (2008) 2-5. ISSN 1211-877X
[7] W.M. Thomas, E.D. Nicholas, Mater. Des. 18 (1997) 269.
[8] B. Tweedy, S. Sellmeyer, A. Jahn, D. Burford, Static Strength Comparison of Riveted versus Friction Stir Welded Stiffened Panels, In: 47th AIAA Conference, Newport, Rhode Island, 2006.
[9] E.D. Nicholas, W.M. Thomas., Int. J. Mater. Prod. Technol. 13(1) (1998) 45.
[10] P. Bělský, Friction Stir Welding of Aircraft Structures, Czech Aerospace Proceedings 3 (2003) 15-17. ISSN 1211-877X.
[11] C.B. Smith, et al., Friction Stir Welding in the Automotive Industry, 2001. Available online: http://www.frictionstirlink.com/publications/Pub07FSWAutoIndTMSPaperpdf.pdf.
[12] P. Cavaliere, G. Campanile, F. Panella, A. Squillace, J. Mater. Process. Technol. 180(1–3) (2006) 263.
[13] R.S. Mishraa, Z.Y. Ma., Mater. Sci. Eng. 50 (2005) 1.
[14] D. Fersini, A. Pirondi, Eng. Fract. Mech. 74 (2007) 468.
[15] C. Zhou, X. Yang, G. Luan, Mat. Sci. Eng. A-Struct. 418 (2006) 155.
[16] M. Ericsson, R. Sandström., Int. J. Fatigue 25 (2003) 1379.
[17] G. Çam, Int. Mater. Reviews 56 (2011) 1.
[18] S. Baragetti, G. D'urso, J. Mech. Sci. Technol. 28(3) (2014) 867.
[19] O. Oosterkamp, L.D. Oosterkamp, A. Nordeide, Weld. J. 83 (2004) 225.
[20] T.L. Dickerson, Int. J. Fatigue 25 (2003) 1399.
[21] Bo Li, Yifu Shen, Weiye Hu, Mater. Des. 32 (2011) 2073.
[22] M. Kadlec, R. Růžek, L. Nováková, Int. J. Fatigue 74 (2015) 1.
[23] AWS D17.3/D17.3M:2010, Specification for Friction Stir Welding of Aluminum Alloys for Aerospace Applications, Miami (USA), American Welding Society, 2009.
[24] EN 6072, Aerospace series: Metallic materials – Test methods, Constant amplitude fatigue testing, AECMA standard, 2010.
[25]V. Richter-Trummer, E. Suzano, M. Beltrão, A. Roos, J.F. dos Santos, P.M.S.T. de Castro, Mat. Sci. Eng. A 538 (2012) 81.